Title: Regional Source-type Discrimination Using Nonlinear Alignment Algorithms

Authors: Marlon D. Ramos, Rigobert Tibi, Christopher J. Young, Erica L. Emry

Author Affiliation(s): Sandia National Laboratories

Corresponding Author Contact Information:

Email: mdramos@sandia.gov

Address: Sandia National Laboratories / Marlon Ramos, Mail Stop 0404 / PO Box 5800 /

Albuquerque, NM 87185

Word Count: 3304/3500

Abstract

The discrimination problem in seismology aims to accurately classify different underground source types based on local, regional or teleseismic observations of ground motion. Typical discriminant approaches are rooted in fundamental, physics-based differences in radiation pattern or wave excitation, which can be frequency dependent and may not make use of the full waveform. In this paper, we explore a new method for event discrimination using phase and amplitude distances derived from dynamic time warping (DTW) and elastic shape analysis (ESA). We demonstrate the ability to distinguish underground point-sources using synthetic waveforms calculated for a 1-D Earth model and various source mechanisms. We then apply the method to recorded data from events in the Korean Peninsula, which includes declared nuclear explosions, a collapse event, and naturally occurring earthquakes. Phase and amplitude distances derived from DTW and ESA are then used to classify the event types via dendrogram and k-nearest neighbor clustering analyses. Using information from the full waveform, we show how different underground sources can be distinguished at regional distances. We highlight the potential of these nonlinear alignment algorithms for discrimination and comment on ways we can extend the framework presented here.

Introduction

Source type discrimination is needed to classify events and develop accurate seismic catalogs. Traditional discriminants exploit physics-based intuition that the radiation pattern of double-couple sources (e.g., earthquakes) should be fundamentally different from explosion-like sources (e.g., chemical/nuclear tests, mining blasts and collapses). This is due to the difference in energy release that exists between shear slip and a pressure pulse acting on the rock (Ben-Menahem and Singh, 1981). Approaches to discrimination between seismic events include moment tensor inversion (Alvizuri and Tape, 2018; Pasyanos and Chiang, 2022), body to surface-wave magnitude ratios (Ms:m_b, Stevens and Day, 1985), spectral amplitude ratios (e.g., Tibi, 2021) and recently, machine learning methods (e.g., Maguire et al., 2024). However, challenges to these methods include isolating source from path and site effects on the waveform, and in the case of machine learning, analysts may not have enough large, labeled datasets to draw from for a given region of interest.

Nonlinear dynamic programming techniques, broadly referred to as dynamic time warping (DTW), have been used to determine what temporal shifts are necessary to optimally align time series (Anderson and Gaby, 1983; Kumar et al., 2022; Müller, 2021). DTW has been applied to seismic exploration (Hale, 2013), ambient-noise interferometry (Mikesell et al., 2015; Yuan et al., 2021) and linear seismic inversion problems (Tan and Langston, 2022). DTW algorithms capture phase variability quite well but may not be as robust to amplitude variability (Müller et al., 2021). This is a concern for seismic event monitoring and especially in the context of signal window selection, which can contain both body and surface waves with markedly different amplitudes. A novel representation of functional data that addresses both phase and amplitude variability within a time series is elastic shape analysis of curves (ESA; Tucker et al., 2013). The ESA method aligns signals to one another after applying a square root slope function (SRSF; Joshi et al., 2007; Srivastava et al., 2011). The SRSF is a distance-preserving transformation between metric spaces (isometry) and yields a proper distance in either phase or amplitude space. Our hypothesis is that two signals sharing the same source mechanism (or, alternatively, the same Green's function) will have a lower phase or amplitude distance whereas signals that do not will have correspondingly higher distances. Moreover, nonlinear alignment methods are data type agnostic and may be applied across monitoring distances or recorded frequencies.

This manuscript explores how nonlinear time series alignment algorithms can assist event type discrimination. First, we set up a synthetic test relevant to regional distance monitoring and demonstrate how DTW and ESA can distinguish double couple from non-double couple (e.g., explosive) signals. We then analyze a seismic dataset of earthquake, explosion, and collapse events in the Democratic People's Republic of Korea (DPRK) and apply hierarchical clustering and k-nearest neighbor (knn) analysis to the DTW and ESA distances. We compare the DTW and ESA methods and discuss recommendations to extend this preliminary analysis.

Methodology

Dynamic Time Warping

DTW estimates time shifts between signals to estimate geophysical parameters and can overcome strong cycle-skipping even in the presence of low signal to noise-ratio (SNR), which is an advantage over windowed cross-correlation and linear trace stretching methods that may estimate incorrect lag times (Mikesell et al., 2015). However, to optimally align signals, unrealistically large dilation of the original time series can occur and strategies to constrain the dynamic programming algorithm (i.e., global or local constraints on the permissible warping function) to reasonable dilation values are not always easy to set a-priori. Despite these choices, DTW allows one to calculate a non-Euclidian distance metric that gives a measure of how much warping was needed for optimal alignment, the DTW distance (*DTW_{dist}*), defined below as,

$$DTW_{dist}(f_1, f_2) = \min\{w_p(f_1, f_2)\} \quad (1)$$

where w_p is the warping path that aligns $f_1(t)$ and $f_2(t)$ after an accumulated distance matrix is computed (Müller, 2021).

Elastic Shape Analysis

An extension and improvement of DTW, ESA separates amplitude and phase information uniquely by first computing the SRSF, $q(t)$,

$$q(t) = sign(f\dot(t))\sqrt{|f\dot(t)|} \quad (2)$$

where $q(t)$ is the transformed signal and $f\dot(t)$ is the first derivative of the original signal with respect to time (Srivistava et al., 2011). The amplitude distance (D_y) between two functions $f_1(t)$ and $f_2(t)$ is defined as,

$$D_y(f_1, f_2) = inf_{\gamma \in \Gamma} \parallel q_1 - (q_2 \circ \gamma)\sqrt{\dot{\gamma}} \parallel \quad (3)$$

where q_1 and q_2 are the SRSF of $f_1(t)$ and $f_2(t)$, respectively, and γ is the warping function that best aligns them. The double-bars "|| ||" denote the L2-norm and Γ represents the complete set of invertible functions that map a smooth surface to each another such that both the function and its inverse are well defined over [0,1]. The phase distance (D_x) is then defined as the distance between warping functions according to,

$$D_x(\gamma_1, \gamma_2) = d_\psi(\psi_1, \psi_2) \equiv \cos^{-1}\left(\int_0^1 \psi_1(t)\psi_2(t)\, dt\right) \tag{4}$$

where ψ(t) represents a mapping of the warping function to Hilbert space ($\mathcal{H}$) and D_x is thus the arc-length between the corresponding SRSF on a $\mathcal{H}$ unit sphere. The theory behind elastic distances is rich, and we refer the interested reader to Wu and Srivastava (2011), Srivastava et al., (2011) or Tucker et al., (2013) for the in-depth, mathematical underpinnings of D_x and D_y. The important properties of ESA are: 1) D_y and D_x are independent of one another, 2) the SRSF transformation guarantees a mathematically proper distance, and 3) the distances are invariant to warping order.

We conceptually show how DTW and ESA align two seismic waveforms in Figure 1. We select data from a single station (DBN08, vertical component) in the Dongbei seismic network (Chun and Richards, 2004). DBN08 recorded both the 2006 and 2009 declared nuclear tests by the DPRK and the P_n and P_g phases are readily identifiable. Because the explosions have different yields and are not exactly co-located (Myers et al., 2018), nonlinear warping must address differences from both the source mechanism and Green's functions. ESA calculates both D_x and D_y (Figure 1B) and DTW yields the DTW_{dist} (Figure 1C). We note that while both techniques result in a better alignment between recorded explosion waveforms (i.e., a higher cross-correlation coefficient), ESA alignment yields a lower cross-correlation coefficient compared to alignment using DTW. However, ESA preserves the original signal length and arrival time difference between P_n and P_g (Figure 1A).

Synthetic and Observed Seismograms

We generate near-regional synthetic seismic waveforms using a 1-D velocity model developed for the DPRK (Ford et al., 2009; Figure 2). We use a wave-number integration algorithm (Herrmann, 2013) to calculate synthetics for double-couple, compensated linear vector dipole (CLVD), explosion, and implosion point-sources recorded at 100 km distance (Figure 2A). We calculate only the down-going Green's function components to suppress strong free-surface effects on the waveform. This lets us simplify and focus our analysis on waveform differences due to source mechanism alone. We filter the 40-samples-per-second synthetic waveforms between 0.5 to 5 Hz (Tibi, 2021) and normalize each trace by its respective maximum amplitude prior to alignment. We also concatenate the vertical (Z) and radial (R) components into a composite time series before warping and alignment to mimic practice in signal detection. Note that for a pure isotropic explosion source, there is no tangential (T) motion generated and thus that component is not considered in the synthetic analysis because discrimination would be trivial.

For the observational dataset, we use waveforms analyzed in Tibi (2021). This dataset contains six declared explosions, fifteen nearby naturally occurring earthquakes and one collapse event following the 2017 declared North Korean nuclear test. Four regional broadband stations are selected from the IC, IU and KS seismic networks. We download waveforms up to 15 minutes after the respective origin time of the events from the Incorporated Research

Institutions for Seismology (IRIS) database to ensure P_n, P_g, and L_g phases are captured, and we filter signals below 10 Hz. Due to different station start and end times, not all events are recorded; also, stations with non-emergent phases are excluded from analysis.

Results

Synthetic Waveform Alignment

We select a double-couple earthquake waveform as the master signal to align to (EQ1, Figure 2A). Each waveform has a P-wave arrival near 15 seconds after the respective event origin time, but to highlight phase arrivals of interest, we cut the waveforms from 15 to 40 seconds for both R and Z components. We calculate DTW_{dist}, D_x and D_y between every signal and EQ1 (Figure 2B, C). We observe that for both DTW and ESA, the distance between EQ1 and itself is zero (expected) and the explosion and implosion events have greater phase and amplitude distances than alignment to the earthquake or CLVD events. This synthetic experiment conceptually demonstrates that if the Green's function is the same, differences due to source mechanism can be inferred via phase or amplitude distance information from DTW and ESA between the full waveforms.

Korean Peninsula Data Analysis

Regional seismic stations recorded the declared 2006 (NK1), 2009 (NK2), 2013 (NK3), 2016 (NK4, NK5) and 2017 (NK6) DPRK nuclear tests, one collapse event following NK6, and explosion-induced aftershocks or isolated, natural seismicity. Tibi (2021) compiled a database of these twenty events and applied a bivariant discriminant function to successfully classify explosion from collapse and earthquake event types. We use a subset of the stations used in

Tibi (2021) to assess DTW and ESA performance on regional distance waveforms (Figure 3A). For any station, the signal time window spans five seconds before theoretically expected P_n and ~40 seconds after the L_g arrival (Figure 3B).

We apply hierarchical clustering analysis to DTW and ESA distances obtained using signals recorded at MDJ in Figure 4. We compute the phase, amplitude and DTW distances between each bandpass filtered (0.5 – 5 Hz) signal pair (Figure 4A, B, C). We also report the cross-correlation between each pair to see where a particular distance metric may align with empirical signal similarity (Figure 4D). We calculate condensed matrix representations of D_x, D_y, and DTW_{dist} and show the results graphically using a dendrogram (Figure 4E, F). We observe that there appears to be more structure in the D_y and DTW_{dist} matrices, based off a qualitative comparison to the cross-correlation matrix.

To assess whether we can achieve better classification between earthquake, explosion and collapse events using both phase and amplitude information, we form a simple linear combination of D_x and D_y following Tucker et al., (2012), using a weighting coefficient, τ. Since D_y appears to have more structure than D_x, we weight D_y more in the below formulation,

$$D_\tau = \tau D_y + (1 - D_x)\tau \qquad (5)$$

To optimize the weighting coefficient τ, we randomly set aside 50% of the signals as training data (Tucker et al., 2012) and employ a Leave-One-Out (LOO) cross-validated knn classifier for varying τ levels ($0 \leq \tau \leq 1$ in an increment of 0.1) in expression (5). We set the value of knn to three because we have exactly three signal types to cluster. Our metric for classification accuracy is the percentage of true predictions returned by knn, based off the signal type labels we assign. We found that τ values between 0.1 – 0.9 classify signal types to the ~70% accuracy level, and we do not observe appreciable changes between τ values to the hundredths decimal point. We only have twenty labeled signals to work with at MDJ, so using a larger signal database (for a given station) could give us more robust statistics. Using either nonlinear alignment methods suggests that the explosion waveforms are separated from earthquake waveforms, but the collapse event may group with either the earthquake (DTW) or explosion (ESA) population. The results shown for MDJ do not dramatically change if the signal envelope is used, or if the R and T component waveforms are concatenated to Z.

We report which ground motion component, signal type, window length and frequency passband that best distinguishes explosion from non-explosion signals for our full set of regional stations in Table 1. The criterion for choosing a particular passband is an improvement in classification accuracy. We list how the LOO cross validation with knn performed for D_x, D_y and DTW_{dist} separately to see if any one distance is superior to another (Table 1). For stations less than 300 km from the source, knn classification using D_y performs comparably to DTW_{dist} and slightly better than D_x. Stations at greater distances (>300 km) from the source (e.g., YSS) do not record waveforms with qualities that are sufficient for this type of analysis (i.e., SNR > 3). This may impact classification accuracy as it is essentially the same between all distance metrics at SEO2 (Table 1). Note also that the relative time window accordingly widens to accommodate larger P to L_g separation time. For the τ analysis at station MDJ, we attempted to find the best linear combination of D_x and D_y that improved classification accuracy, but ultimately found that D_y by itself is superior, which may not be the case for every dataset. Moreover, there is no reason to stick to a linear relationship between the phase and amplitude distance matrices and this assumption may be relaxed in future work. For most of the signals analyzed here, there is little improvement in accuracy between the signal waveforms compared to the envelope functions (at least for the frequency bands considered here), but this deserves further exploration.

Discussions and Conclusion

Method Sensitivity

We conceptually showed how nonlinear warping distances can distinguish dissimilar signal types using synthetics, and when we applied advanced clustering on the actual data, we saw that modest classification accuracies can be achieved. This result may stem from complex wave propagation that is generally not captured when using a 1-D or laterally homogenous earth model but is certainly present in the real Earth. Differences between source types can be deduced from narrowband filters, as is commonly used in P_g/L_g ratio analyses (Pyle and Walter, 2021; Tibi et al., 2023). Similarly, the selection of an appropriate filtering passband, SNR, and consequently, time window length was central to our analysis. For MDJ, we analyzed several frequency passbands to capture lower-frequency L_g (< 1Hz) or higher frequency P (> 2 Hz). All signal types from this dataset were present at MDJ, and our clustering approach is most accurate for this station. However, we acknowledge that this is a small, imbalanced dataset and future work should target a labeled database of diverse source types with varying SNR so that the DTW/ESA framework can be further assessed in comparison to neural network classifiers (e.g., Eggertsson et al., 2024; Maguire et al., 2024) or other discrimination approaches.

Recently, focal depth discriminants have been developed at local-to-regional distances that use differential magnitudes or spectral amplitude ratios (i.e., R_g/S_g, P_g/S_g) between mine blasts and earthquakes (Koper et al., 2024). In this study, the depth was held constant in the synthetic experiment (1 km) and was 5-km and shallower for the DPRK dataset. There is opportunity to extend the nonlinear alignment framework for depth discrimination as well since focal depth differences can influence body and surface wave excitation (Zhang et al., 2002).

DTW has been shown to align time series even if there is significant noise present (Mikesell et al., 2015) but there is potential to mis-align desired signal to noise. Moreover, the ambient-noise interferometry application of DTW is different than discrimination and data processing choices may differ. Because ESA defines the signal shape space such that proper distance metrics can be calculated, robust statistics can be applied to extract physically meaningful clusters of data. Furthermore, the centrality of functions in D_x and D_y space can now be measured using elastic depths, which have been shown to detect outliers in functional data (Harris et al., 2020). This new technique can be applied to the discrimination problem at various monitoring distances.

Optimal Signal Separation and Monitoring Implications

Previous studies have shown that for ESA, either amplitude or phase distance can perform better for a particular signal classification application (Tucker et al., 2014) and linear combinations of them can provide better results than using either one alone. Using MDJ as an example, we saw that D_y by itself and the joint combination of D_y and D_x had a greater classification accuracy than D_x (Table 1, Figure 4). Why might that be? It could be due to the higher relative P_n and P_g amplitudes on the explosion waveforms, which are present across a wide frequency band. Alternatively, it may be due the complexity of phase information between these source types which suggests phase-based metrics alone may not offer a simple interpretation. We are also interested is the relationship between cross-correlation coefficient and phase or amplitude distance, as well. We showed that a given distance matrix has an inverse relationship to the similarity matrix, consistent with our hypothesis that any two highly similar signals will have a smaller distance between them in phase or amplitude spaces (Figures 2 and 4). ESA could be adapted to assist empirical cross-correlation signal detection by extending the correlation range of templates to account for small differences in source mechanism or Green's function. One of the biggest shortcomings of standard correlation detectors is the curation of an optimal template library and appropriate detection statistic (Gibbons, 2022). We believe automatic event screening could leverage one (or more) signal distance spaces to address this issue.

We have shown that nonlinear alignment techniques such as DTW or ESA can discriminate signal types, with special consideration to frequency content, time-window, and component analyzed. Low magnitude events may be difficult to classify due to their lower SNR when regional distance stations are used. The potential advantage of the discriminant method we presented here is that one can use the full waveform, increasing the available time bandwidth product. Possible future directions include examining the transportability of this discriminant method using a larger regional dataset, systematic evaluation of how monitoring distance and frequency passband influence the results, and an exploration into how additional source information can be inferred from phase or amplitude distance metrics (i.e., yield, hypocenter depth/depth-of-burial).

Data and Resources

To replicate our workflow, the *Computer Programs in Seismology* (CPS) software must be compiled (installation here: https://www.eas.slu.edu/eqc/eqccps.html). Earthquake, collapse, and explosion waveforms are freely accessible through the IRIS data web-service (last accessed on May 10, 2024). Maps are made using the PyGMT software (Uieda et al., 2023).

Declaration of Competing Interests

The authors acknowledge that there are no conflicts of interest recorded.

Acknowledgements

This Ground-based Nuclear Detonation Detection (GNDD) research was funded by the National Nuclear Security Administration, Defense Nuclear Nonproliferation Research and Development (NNSA DNN R&D). Sandia National Laboratories is a multimission laboratory managed and operated by National Technology & Engineering Solutions of Sandia, LLC, a wholly owned subsidiary of Honeywell International Inc., for the U.S. Department of Energy's National Nuclear Security Administration under Contract Number DE-NA0003525. ChatGPT, or any variation thereof, was not used to write any part of this manuscript. We thank Derek Tucker for discussions on the application of Elastic Shape Analysis and Bob Herrmann for assistance with CPS.

References

Alvizuri, C., and C. Tape (2018). Full moment tensor analysis of nuclear explosions in North Korea. *Seis. Res. Lett.*, 89(6), 2139–2151. https://doi.org/10.1785/0220180158.

Anderson, K. R. and J. E. Gaby (1983). Dynamic Waveform Matching. *Information Sciences*, 31, 221 – 242.

Ben-Menahem, A. and Singh, S.J. (198). Seismic Waves and Sources, Springer Verlag, New York, NY.

Chun, K-Y and P. G. Richards (2004). *Dongbei Broadband Network* [Data set]. International Federation of Digital Seismograph Networks. https://doi.org/10.7914/SN/5G_2004.

Eggertsson, G., Lund, B., Roth, M., and Schmidt, P. (2024). Earthquake or blast? Classification of local-distance seismic events in Sweden using fully connected neural networks, *Geophys. Jour. Int.*, 236, 1728 – 1742, doi.org/10.1093/gji/ggae018.

Ford, S. R., D. S. Dreger, and W. R. Walter (2009). Source Analysis of the Memorial Day explosion, Kimcaek, North Korea, *Geophys. Res. Lett.,* 36, L21304, doi:10.1029/2009GL040003.

Gibbons, S. J. (2022). The optimal correlation detector?, *Geophys. Jour. Int.*, 228, 355 – 365, doi.org/10.1093/gji/ggab344.

Hale, D. (2013). Dynamic warping of seismic images, *Geophys.*, 78(2), S105–S115.

Harris, T., Tucker, D. J., Li, B., and Shand, L. (2020). Elastic Depths for Detecting Shape Anomalies in Functional Data, *Technometrics,* 00, 1 – 11, doi:10.1080/00401706.2020.1811156.

Herrmann, R. B. (2013). Computer programs in seismology: An evolving tool for instruction and research, *Seism. Res. Lettr.* **84**, 1081-1088, doi:10.1785/0220110096.

Joshi, S.H., E. Klassen, A. Srivastava, I. H. Jermyn (2007). A novel representation for Riemannian analysis of elastic curves in Rn, *Proceedings of IEEE CVPR*. pp. 1–7.

Kumar, U., C. P. Legendre, L. Zhao, and B. F. Chao (2022). Dynamic time warping as an alternative to windowed cross correlation in seismological applications, *Seismological Research Letters*, 93(3), 1909–1921. doi: 10.1785/0220210288.

Maguire, R., B. Schmandt, R. Wang, Q. Kong, and P. Sanchez (2024). Generalization of Deep-Learning Models for Classification of Local Distance Earthquakes and Explosions across Various Geologic Settings, *Seismol. Res. Lett*. XX, 1–10, doi: 10.1785/ 0220230267.

Mikesell, T. D., A. E. Malcolm, D. Yang and M. H. Haney (2015). A comparison of methods to estimate phase delays: numerical examples for coda wave interferometry, *Geophysical Journal International*, 202, 347 – 360, doi: 10.1093/gji/ggv138.

Müller, M. (2021). Fundamentals of music processing using Python and Jupyter notebooks, *Springer,* doi:10.1007/978-3-030-69808-9.

Myers, S. C., S. R. Ford, R. J. Mellors, S. Baker, and G. Ichinose (2018). Absolute locations of the North Korean nuclear tests based on differential seismic arrival times and InSAR. *Seismological Research Letters*, 89(6), 2049–2058. https://doi.org/10.1785/0220180123.

Pasyanos, M. E. and A. Chiang, (2022). Full moment tensor solutions of U.S. underground nuclear tests for event screening and yield estimation, *Bull. Seis. Soc. of Amer.*, 112, 538–552.

Pyle, M. L., and W. R. Walter (2021). Exploring the Effects of Emplacement Conditions on Explosion P/S Ratios across Local to Regional Distances, *Seismol. Res. Lett*. 93, 866–879, doi: 10.1785/0220210270.

Srivastava, A., E. Klassen, S. Joshi, and I. Jermyn (2011). Shape analysis of elastic curves in Euclidean spaces. *IEEE Transactions on Pattern Analysis and Machine Intelligence* 33 (7), 1415–1428.

Stevens, J. L. and S. M. Day (1985). The physical basis of mb: MS and variable frequency magnitude methods for earthquake/explosion discrimination. *Journal of Geophysical Research*, 90, 3009–3020.

Tan, J., and C. A. Langston (2022). Shape Dynamic Time Warping for Seismic Waveform Inversion, *Bulletin of the Seismological Society of America*, XX, 1–18, doi: 10.1785/0120220051.

Tibi, R. (2021). Discrimination of Seismic Events (2006– 2020) in North Korea Using P/Lg Amplitude Ratios from Regional Stations and a Bivariate Discriminant Function, *Seismol. Res. Lett.* 92, 2399–2409, doi: 10.1785/0220200432.

Tibi, R., N. Downey, and R. Brogan (2023). Testing and Design of Discriminants for Local Seismic Events Recorded during the Redmond Salt Mine Monitoring Experiment, *Bull. Seismol. Soc. Am.* 114, 906–923, doi: 10.1785/0120230193.

Tucker J. D., Wu, W., and Srivastava, A (2013). Generative models for functional data using and amplitude separation, *Comp. Stats. and Data Analysis* 61, 50 – 66, doi:10.1016/j.csda.2012.12.001.

Tucker, J. D., W. Wu, and A. Srivastava (2014). Analysis of signals under compositional noise with applications to SONAR data, *IEEE Journal of Oceanic Engineering*, vol 29, no. 2. pp 318-330.

Uieda, L., Tian, D., Leong, W. J., Schlitzer, W., Grund, M., Jones, M., et al. (2023). PyGMT: A Python interface for the Generic Mapping Tools. (v0.9.0) [Software]. Zenodo. https://doi.org/10.5281/zenodo.7772533.

Walter, W. R., D. A. Dodge, G. Ichinose, S. C. Myers, M. E. Pasyanos, and S. R. Ford (2018). Body-wave methods of distinguishing between explosions, collapses, and earthquakes: Application to recent events in North Korea, *Seismol. Res. Lett*. 89, 2131–2138.

Yuan, C., J. Bryan, and M. Denolle (2021). Numerical comparison of time-, frequency- and wavelet-domain methods for coda wave interferometry, *Geophysical Journal International*, 226(2), 828–846, doi: 10.1093/ GJI/GGAB1.

Zhang, J., T. Lay, J. Zaslow, and W. R. Walter (2002). Source effects on regional seismic discriminant measurements, *Bull. Seismol. Soc. Am*. 92, 2926–2945.

Author Mailing Address

1. Marlon D. Ramos
2. Rigobert Tibi
3. Christopher J. Young
4. Erica L. Emry

Sandia National Laboratories
1515 Eubank Blvd. SE
Albuquerque, NM 87123

Tables

Table 1: Hierarchical Clustering Results for Regional Seismic Stations. Note that due to data availability issues or low SNR, not all events are included at a particular station.

Station	Component(s)	Signal Type	Events Included	Source Receiver Distance (km)	Window Length (sec)	Filter band (Hz)	% Accuracy (Dx)	% Accuracy (Dy)	% Accuracy (DTWdist)
SEHB	BHN	Envelope	EQ1, EQ2, EQ7, NK5, NK6, CO	344.1	100	0.8 – 8.0	33	50	50
MDJ	BHZ	Waveform	EQ1, EQ2, EQ3, EQ4, EQ5, EQ6,	371.0	100	0.5 – 5.0	65	90	90
SEO2	BHN	Waveform	EQ1, EQ2, EQ3, EQ9, EQ10, EQ11	461.8	120	0.8 – 6.0	67	67	67
YSS	BHZ	Waveform	EQ2, NK4, NK4, NK5, NK6, CO	1256.6	440	0.5 – 6.0	N/A	N/A	N/A

Net work	KS	IC	KS	IC

List of Figures Captions

Figure 1. Illustrative example of nonlinear alignment algorithms applied to explosions (vertical component) recorded at DBO8, a station belonging to the Dongbei Seismic Network. A) Normalized, filtered signals (3-pole, zero-phase, 0.5 – 2 Hz Butterworth) from the NK1 and NK2 nuclear tests and aligned signals using ESA and DTW are shown. A metric for similarity, the maximum cross-correlation coefficient (CC), is tabulated before and after alignment. P_n *and* P_g *seismic phase arrivals are labeled by the solid and dashed vertical lines, respectively. B) The ESA warping function plotted through time between NK1 and NK2. The elastic phase (Dx) and amplitude (Dy) distance are given in the upper lefthand corner. C) The warping path (*W_p*) between NK1 and NK2 using DTW without constraints.* W_p *is superposed over the base ten logarithm of the accumulated distance matrix (D). The DTW distance (*DTW_{dist}*) is given in the upper righthand plot. NK1 and NK2 denote the 9 October 2006 01:35:28.00 and 25 May 2009 00:54:43.12 nuclear tests, respectively (Table 1 in Tibi, 2021).*

Figure 2. A) Concatenated vertical (Z) and radial (R) component synthetics calculated for the Ford et al. (2009) velocity model recorded at a source-receiver distance of 100 km assuming an azimuth of 30 degrees and hypocenter depth of 1 km. Source mechanisms range from purely double-couple (bottom) to implosive (top) sources. The waveforms are normalized to their respective maximum amplitude and distinct phase arrival times are denoted by thin gray lines on Z components. Direct P and S are labeled. B) Dynamic time warping distance (DTW_{dist}*) between each waveform pair relative to EQ1, normalized by the largest* DTW_{dist}*. C) Elastic phase (Dx) and amplitude (Dy) distances for each warping pair (unnormalized). Legend in C applies to subfigures B and C.*

Figure 3. A) Map of DPRK and surrounding region showing seismic stations used in the cluster analysis. Average epicenter of the NK1 - NK6 tests, collapse event, and naturally occurring earthquakes is denoted by the red star. B) Example vertical-component waveforms of an explosion, collapse and earthquake event recorded at station MDJ (network IC). National Earthquake Information Center body-wave magnitudes (m_b*) tabulated on the righthand side*

of the plot. Filter passband is between 0.5 – 5 Hz. A group velocity of 3.6 km/s is assumed to estimate the L_g arrival whereas the PREM earth model is used to calculate P_n and P_g arrival times.

Figure 4. Cluster analysis at station MDJ. Indices along the axes in (A)-(D) are as follows: 0 – 12 (earthquake), 13 – 18 (explosion) and 19 (collapse. A) Phase distance, B) amplitude distance, C) DTW distance, and D) maximum cross-correlation coefficient between every earthquake, explosion and collapse signal pair. The diagonal of each symmetric distance matrix is zero or one. E) and F) show the dendrogram trees from hierarchical cluster analysis for ESA and DTW, respectively.

Figures

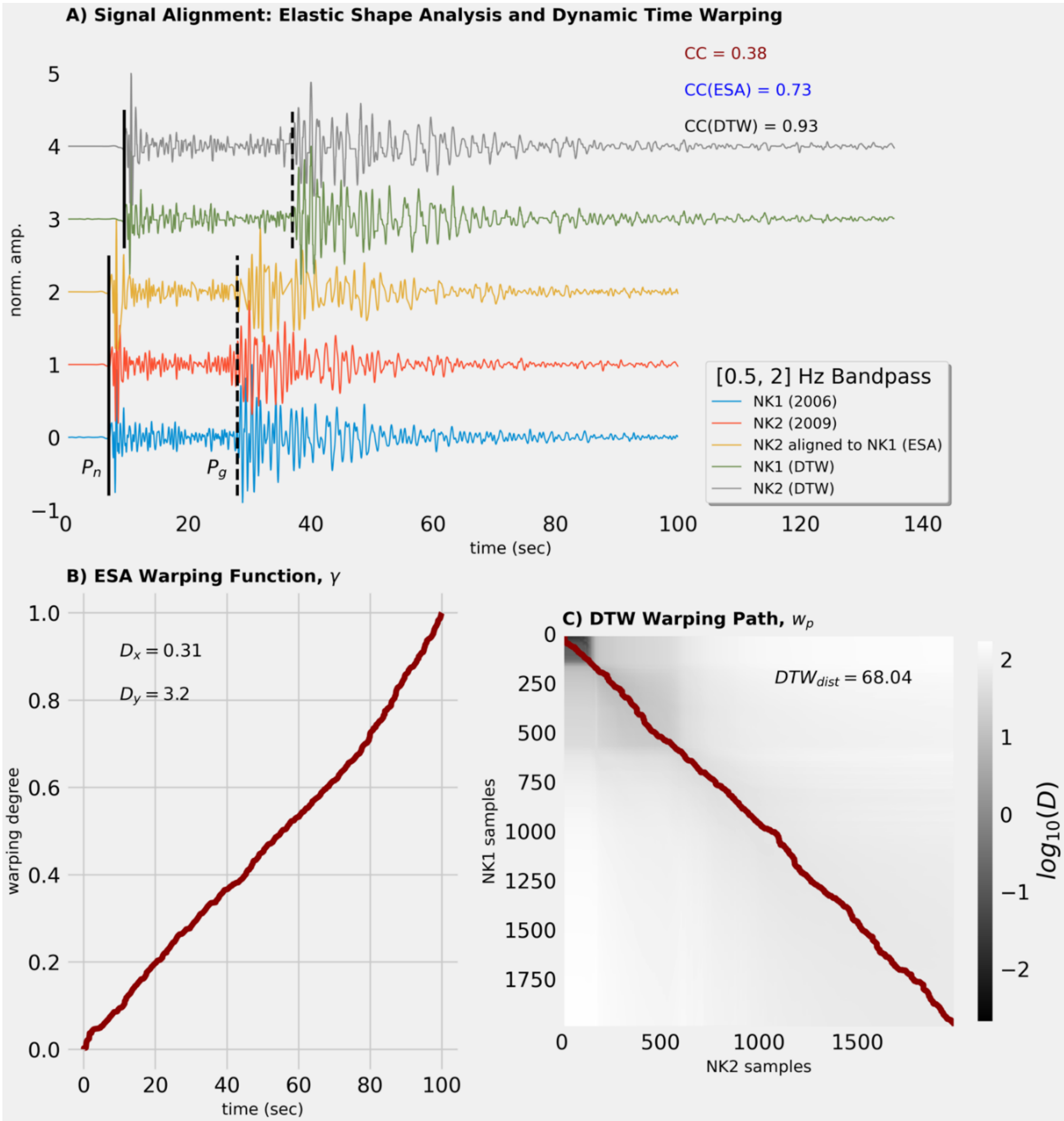

Figure 1. Illustrative example of nonlinear alignment algorithms applied to explosions (vertical component) recorded at DBO8, a station belonging to the Dongbei Seismic Network. A) Normalized, filtered signals (3-pole, zero-phase, 0.5 – 2 Hz Butterworth) from the NK1 and NK2 nuclear tests and aligned signals using ESA and DTW are shown. A metric for similarity, the maximum cross-correlation coefficient (CC), is tabulated before and after alignment. P_n and P_g seismic phase arrivals are labeled by the solid and dashed vertical lines, respectively. B) The ESA warping function plotted through time between NK1 and NK2. The elastic phase (Dx) and amplitude

(Dy) distance are given in the upper lefthand corner. C) The warping path (W_p) between NK1 and NK2 using DTW without constraints. W_p is superposed over the base ten logarithm of the accumulated distance matrix (D). The DTW distance (DTW_{dist}) is given in the upper righthand plot. NK1 and NK2 denote the 9 October 2006 01:35:28.00 and 25 May 2009 00:54:43.12 nuclear tests, respectively (Table 1 in Tibi, 2021).

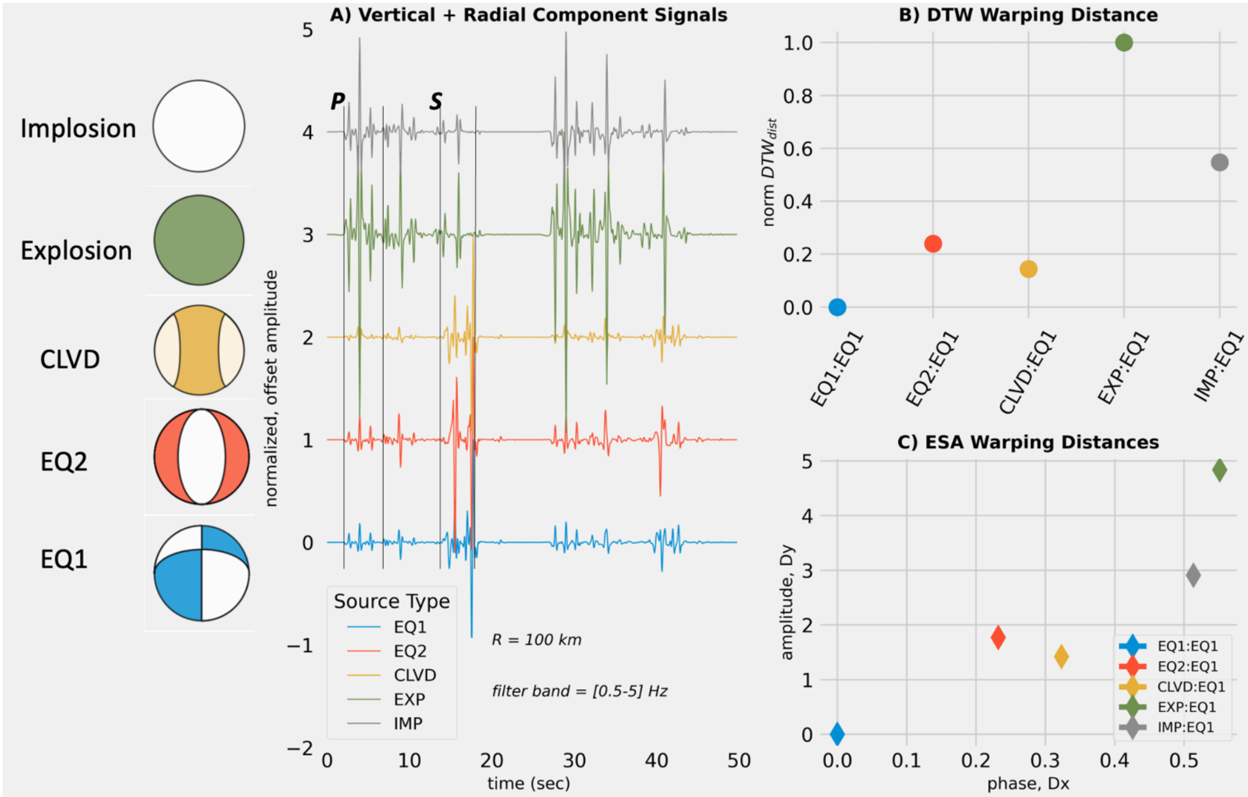

Figure 2. A) Concatenated vertical (Z) and radial (R) component synthetics calculated for the Ford et al. (2009) velocity model recorded at a source-receiver distance of 100 km assuming an azimuth of 30 degrees and hypocenter depth of 1 km. Source mechanisms range from purely double-couple (bottom) to implosive (top) sources. The waveforms are normalized to their respective maximum amplitude and distinct phase arrival times are denoted by thin gray lines on Z components. Direct P and S are labeled. B) Dynamic time warping distance (DTW_{dist}) between each waveform pair relative to EQ1, normalized by the largest DTW_{dist}. C) Elastic phase (Dx) and amplitude (Dy) distances for each warping pair (unnormalized). Legend in C applies to subfigures B and C.

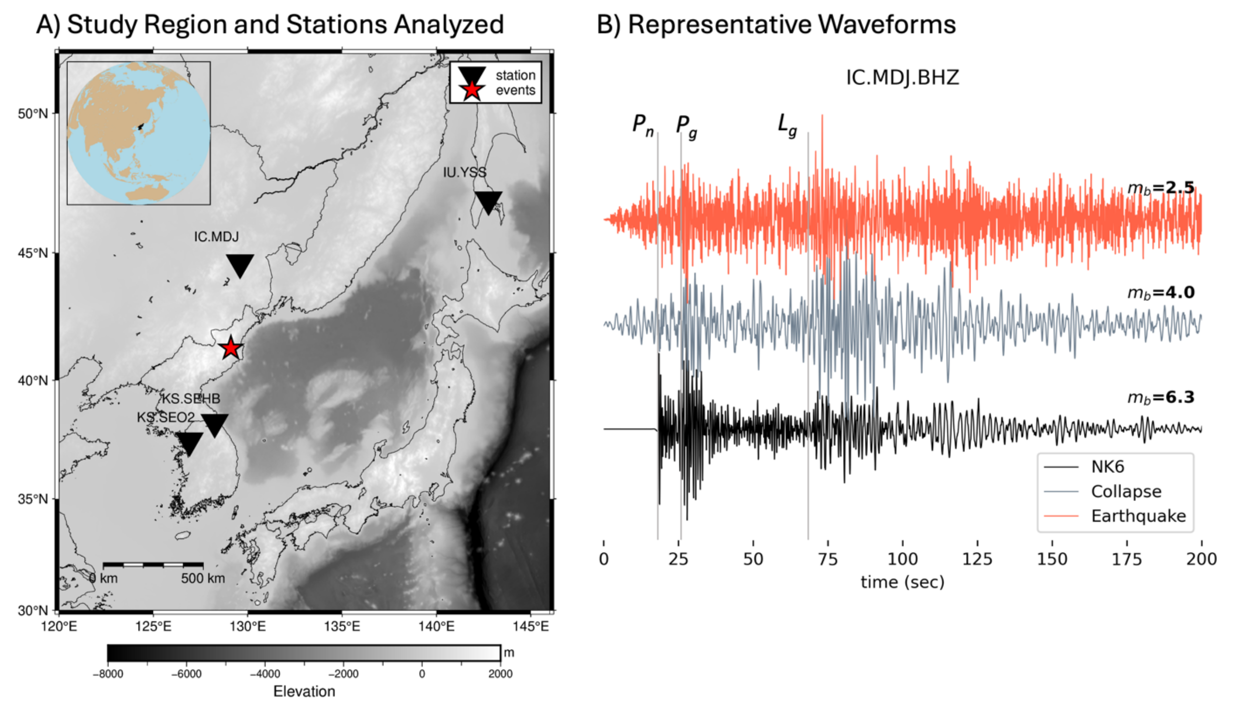

Figure 3. A) Map of DPRK and surrounding region showing seismic stations used in the cluster analysis. Average epicenter of the NK1 - NK6 tests, collapse event, and naturally occurring earthquakes is denoted by the red star. B) Example vertical-component waveforms of an explosion, collapse and earthquake event recorded at station MDJ (network IC). National Earthquake Information Center body-wave magnitudes (m_b) tabulated on the righthand side of the plot. Filter passband is between 0.5 – 5 Hz. A group velocity of 3.6 km/s is assumed to estimate the L_g arrival whereas the PREM earth model is used to calculate P_n and P_g arrival times.

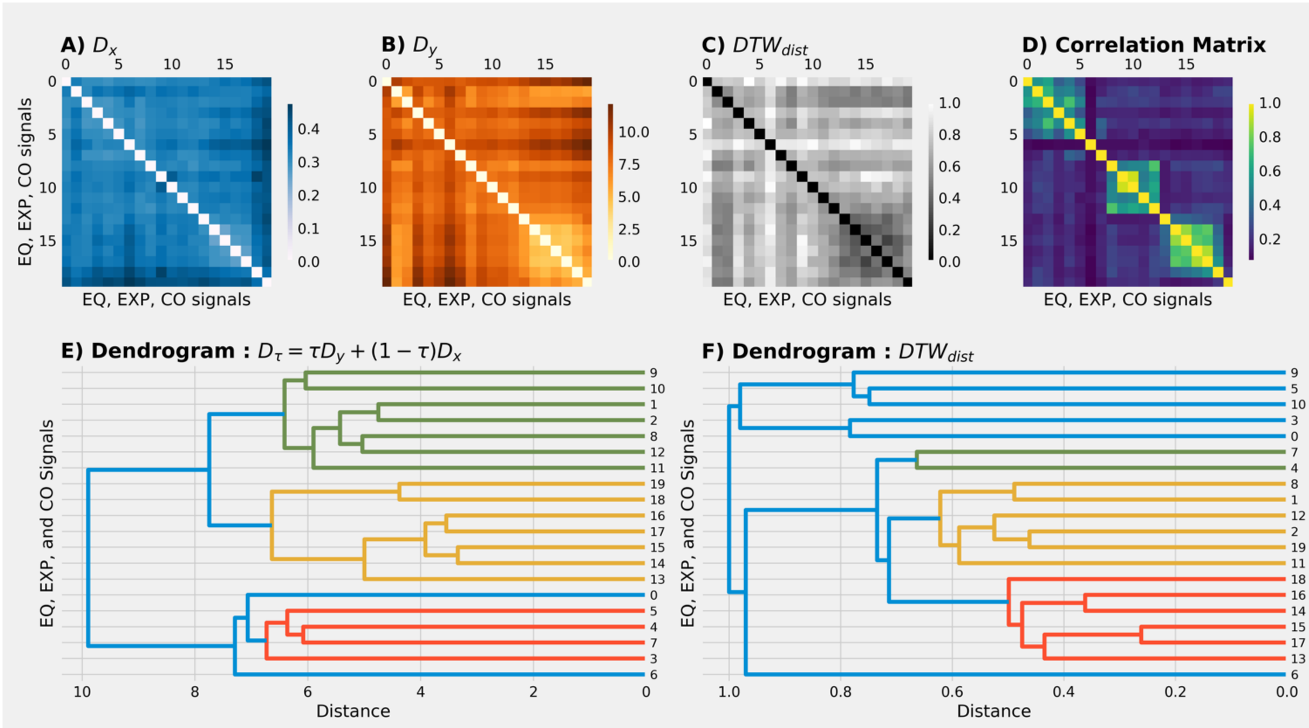

Figure 4. Cluster analysis at station MDJ. Indices along the axes in (A)-(D) are as follows: 0 – 12 (earthquake), 13 – 18 (explosion) and 19 (collapse). A) Phase distance, B) amplitude distance, C) DTW distance, and D) maximum cross-correlation coefficient between every earthquake, explosion and collapse signal pair. The diagonal of each symmetric distance matrix is zero or one. E) and F) show the dendrogram trees from hierarchical cluster analysis for ESA and DTW, respectively. In E), a value of 0.5 is used for the coefficient τ.